Heterogeneous Modeling of Biological Organs and Organ Growth

Roman Ďurikovič[1,2], Silvester Czanner[3], Július Parulek[2,5], and Miloš Šrámek[2,4]

[1] University of Saint Cyril and Metod, Trnava, Slovakia,
[2] Faculty of Mathematics, Physics and Informatics, Comenius University, Slovakia
roman.durikovic@fmph.uniba.sk
[3] Warwick Manufacturing Group, University of Warwick, UK
S.Czanner@warwick.ac.uk
[4] Austrian Academy of Sciences, Austria
[5] Institute of Molecular Physiology and Genetics, Slovak Academy of Sciences, Slovakia

Abstract. The growth of the organs of human embryo is changing significantly over a short period of time in the mother body. The shape of the human organs is organic and has many folds that are difficult to model or animate with conventional techniques. Convolution surface and function representation are a good choice in modelling such organs as human embryo stomach and brain. Two approaches are proposed for animating the organ growth: First, uses a simple line segment skeleton demonstrated on a stomach model and the other method uses a tubular skeleton calculated automatically from a 2D object outline. The growth speed varies with the position within the organ and thus the model is divided into multiple geometric primitives that are later glued by a blending operation. Animation of both the embryo stomach and brain organs is shown.

1 Introduction and Previous Works

The purpose of this manuscript is to model the outer shape and the shape metamorphosis during the growth of some human embryo organs, particularly brain and digestive system. Popular methods like 3D shape reconstruction from Computer Tomography (CT) sections or ultrasound data can not be used for this type of modelling because the resolution of the devices used in those methods are much higher comparing to the size of human embryo. Four weeks old embryo is approximately 3 mm tall while the CT resolution is 1 mm giving us only three sections for a reconstruction process. Usually, the microscopic cross-sections are used to reconstruct the polygonal representation of an embryo, which is exact but complicated process. In case of such destructive approach often a mouse embryo is used instead of the human embryo [1]. To control the shape metamorphosis between two mesh objects become a problem when they have different topology and geometry. To create the realistically looking human organ models and to

A. Pasko, V. Adzhiev, and P. Comninos (Eds.): HOMA, LNCS 4889, pp. 239–258, 2008.

generate the animations demonstrating the growth process requires a proposed methodology.

Growing human organs can be described as dynamical systems with a dynamical structure [2]. In such systems not only the values of variables characterizing system components, but also the number of components and the connections between them, may change over time. There is a need to construct a mathematical description of a system. The model can then be used for simulation or optimization. All models are predictive in the meaning that simulation output predict what could occur in the real world where the system is operating. Numerous interdisciplinary research initiatives are generating excellent research results with regards to modelling, simulation and visualization of human anatomy and physiology. These research initiatives focus on different (biological) levels [3]; molecular and cellular levels, tissue [4] and organ levels [5], [6], [7], and system and human (organism) levels.

The simulation of human organs growing can be seen as an imitation of the reality for studying the effect of changing parameters in a model as a means of preparing a decision or predicting experiment results. Since the human body is mainly made up of a variety of organs, the medical consequence of organ modelling is very important, ranging from heart surgery to minimally-invasive surgery.

In the area of modelling and simulation of human organs many research works have been carried out. One class of reconstruction methodologies uses implicit functions. They allow extracting an iso-surface either by a procedural method, or skeletal implicit surfaces (surfaces generated by a field function and a skeleton). Amrani introduced a method using the skeleton-based implicit surface for implicit reconstruction [7].

Another construction method is presented by Leymarie. His approach is based on propagation along the scaffold from initial sources of flow as a means to efficiently construct it. The detection of these sources can be shown to be reduced to considering pairs of input points, which then constitutes the computational bottleneck of this method [8].

A semi-automatic reconstruction method that can be used on noisy scattered points of a medical organ is presented by Tsingos [5]. The method is based on implicit iso-surfaces generated by skeletons that provide a smooth and compact representation of the surface. The user can guide the reconstruction by initializing some skeletons and their reconstruction windows, thus taking benefits of his initial knowledge of the data.

The method developed by Attali *et al.* [9] computes the Voronoi graph of the point set to build the skeleton of the object and reconstructs its surface. The surface thus reconstructed has only fixed topological type.

Even though the convolution surfaces provide nice blending between several parts of organs, the control of the blend shape is very limited. The functional representation [10] is a tool that generalize the set theoretic operations and generates full range of shapes from simple object union to smooth blend. The animation of such surfaces follow the changes smoothly, even if the topol-

ogy changes. Because of this advantage the functional representation become a popular tool where the shapes to be modelled are from the natural world. We explain here our modelling experience that can be useful for others.

2 Shape Representation for Growth Animation

The polygonal models can not capture the development of such complex process as the growth of the digestive system. So far, we have created the skeletons of different physiological parts, we need to blend them together to get the smooth shapes. Even though, the convolution surfaces provide nice blending between several parts of organs, the control of the blend shape is very limited. The functional representation is a tool that generalizes the set theoretical operations and generates full range of shapes from simple object union to smooth blending. The animation of such surfaces follow the changes smoothly, even if the topology changes. Because of this advantage the *functional representation* is an excellent tool when the shapes to be modelled are from the natural world. We discuss herein the shape modeling based on skeleton calculated from dynamic simulation and L-system growth.

An *implicit surface* is defined by an isosurface of some potential field $F : \mathcal{R}^3 \rightarrow \mathcal{R}$ at threshold level T: $S = \{p \in \mathcal{R}^3 : F(p) - T = 0\}$. The function $F(p)$ is also called an implicit function. A convolution surface is implicitly defined by a potential function F obtained via convolution operator between a kernel and all the points of a skeleton. The convolution surface thus obtained is a smoothed skeleton. The skeleton is a collection of geometric primitives such as point, line segment, arc and plane that outline the structure of an object being modelled. Convolution surface build from complex skeletons can be evaluated individually by adding the local potentials for each primitive, because convolution operator is linear.[3] Let us have N skeleton primitives the above statements can be written as the following modelling equation in an implicit form:

$$\sum_{i=1}^{N} F_i(x_1, x_2, x_3) - T = 0, \tag{1}$$

where F_i is the source potential of i-th skeleton primitive and T is the isopotential threshold value.

3 Function Representation

Let us consider closed subsets of n-dimensional Euclidian space E^n with the definition:

$$f(x_1, x_2, ..., x_n) \geq 0,$$

where f is a real continuous function defined on E^n. The above inequality is called a function representation (F-rep) of a geometric object and function f is called the defining function. In three-dimensional case the boundary of such

a geometric object is called implicit surface. The major requirement on the function is to have at least C^0 continuity. The set of points $X_i(x_1, x_2, ..., x_n) \in E^n$, $i = 0, ..., N$ associated with Eq. 3 can be classified as follows:

$$f(X_i) > 0 \text{ if } X_i \text{ is inside the object,}$$
$$f(X_i) = 0 \text{ if } X_i \text{ is on the boundary of the object,}$$
$$f(X_i) < 0 \text{ if } X_i \text{ is outside the object.}$$

Let us consider from now on the defining function given by the convolution operator between a kernel and all the points of a skeleton, i.e. function F as defined in the last equation of the previous section.

3.1 Set-Theoretic Operations

The binary operations on geometric objects represented by functions can be also defined in the form of function representation by

$$\mathcal{F}(f_1(X), f_2(X)) \geq 0, \tag{2}$$

where $\mathcal{F}$ is a continuous real function of two variables .[10] Such operations are closed on the set of function representations. After set theoretic operation between two subjects defined by functions f_1 and f_2 the resulting object has the defining function as follows:

– For object union

$$f_3 = f_1|f_2 \equiv \frac{1}{1+a}(f_1 + f_2 + \sqrt{f_1^2 + f_2^2 - 2af_1f_2}),$$

– for object intersection

$$f_3 = f_1\&f_2 \equiv \frac{1}{1+a}(f_1 + f_2 - \sqrt{f_1^2 + f_2^2 - 2af_1f_2}),$$

– for object subtraction

$$f_3 = f_1\backslash f_2 \equiv f_1\&(-f_2),$$

where $|, \&, \backslash$ are notations of so-called R-functions and parameter $a = a(f_1, f_2)$ is the arbitrary continuous function satisfying the conditions

$$-1 < a(f_1, f_2) \leq 1$$
$$a(f_1, f_2) = a(f_2, f_1) = a(-f_1, f_2) = a(f_1, -f_2).$$

Please, note that even thought the resulting defining function for set above theoretic operations is continuous, the resulting object is not continuous in general.

3.2 Blending Union Operation

Intuitively the blending union operation between two initial objects from the set of function representations is a gluing operation. It allows us to control the gluing type in the wide range of shapes from pure set union to convolution like summation of terms. Mathematically the blending union operation is defined by

$$\mathcal{F}(f_1, f_2) = f_1 + f_2 + \sqrt{f_1^2 + f_2^2} + \frac{a_0}{1 + (\frac{f_1}{a_1})^2 + (\frac{f_2}{a_2})^2},$$

where f_1 and f_2 are functions representing objects that are blended. The absolute value a_0 defines the total displacement of the bending surface from two initial surfaces. The values $a_0 > 0$ and $a_1 > 0$ are proportional to the distance between blending surface and the original surface defined by f_1 and f_2, respectively. The effect of this operation compared to other possible object connections is demonstrated on two object primitives whose skeleton consists of two line segments one vertical and the other one diagonal, see Figure 1 top-left. Simple plus operation between convolution functions deforms the thickness of vertical convolution cylinders as shown in top-right image. Considering four line segments as a single skeleton of geometric primitive results in the shape shown in top-center image. The sequence of shapes shown on bottom of Figure 1 are the blending union operations between two parallel geometric primitives. The geometric primitives and their skeletons do not change but the blending parameters used to blend them are different for each image. In orderer from left side the used parameters are $a_i = 0.01$, $a_i = 0.07$, $a_i = 0.3$, $a_i = 0.5$, and $a_i = 0.7$, respectively. We can conclude that in the case when the shape and size of geometric primitives must be preserved the blending union operation with different parameters a_0, a_1, and a_2 is a good choice. On the other hand when the blending shape is main concern the convolution plus operation should be used. When both the shape of geometric primitives and that of blending are important the small values of blending union parameters is a choice. The F-rep blending union operation has similar advantages as simple convolution union with respect to minimizing unwanted bulges.

4 Shape of Organic Models

In previous sections have been discussed the theory of F-rep and convolution surfaces. As next, we will show a method to model the organic shapes by F-rep, where each of the geometric primitives is defined by

$$\sum_{i=1}^{N} F_i(x_1, x_2, x_3) - T = 0,$$

where F_i are the source potentials of skeleton primitives i.e. points, lines or triangles and T is a threshold value. Therefore, what we need to design next are the skeletons for different organs.

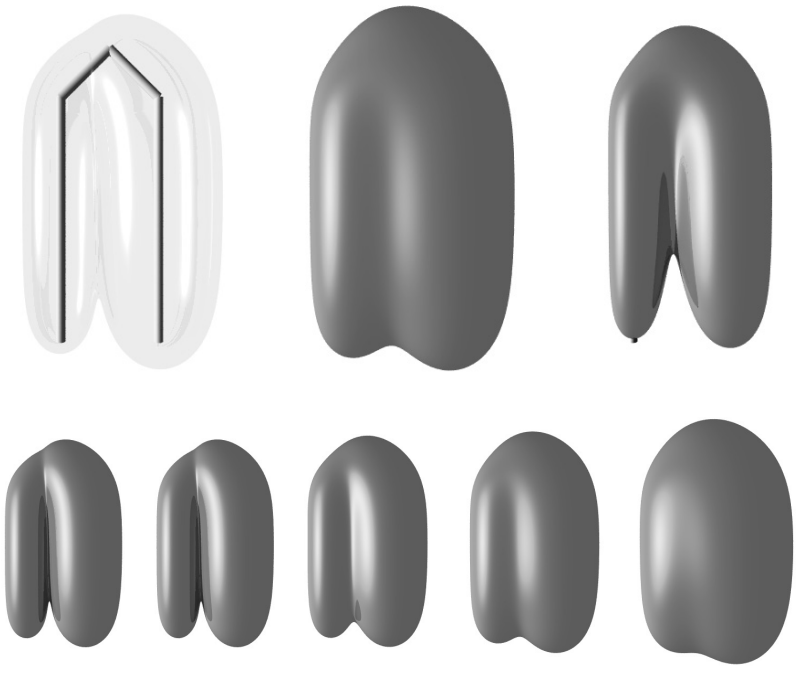

Fig. 1. Blending union operation. top: standard and bottom: Blending union operation.

4.1 Human Brain Model

First step in the model creation process is to obtain the size measurements of brain and stomach stages from atlas of embryology. Embryological atlas contains hand-drawing pictures and photographs of human embryo organs ordered by age. For the purpose of this study the models from 28 - 56 days old brain were used. The brain pictures has been scanned, stored in binary form and measured by ruler. The model, at this stage of precessing, was divided into physiological parts to suite the animation purposes. The outlines of physiological parts were drawn over the pictures and photographs, see Figure 2.

4.2 Brain: Central Skeleton

The result of the measurements is a 2D planar contour, call *the central skeleton*, nearly outlining the outer contour of the shape. Interior of central skeleton is triangulated such that it crates a triangular strip. One can observe different growth speed for different pars of embryo brain. It is therefore natural to divide the central skeleton into those parts. Additional parts could be necessary to model the folds and control the unwanted blending problem near the folding areas. Figure 3, shows namely the part I corresponding to the part of brain called rhombencephalon, part II will develop to mesencephalon and part III is a

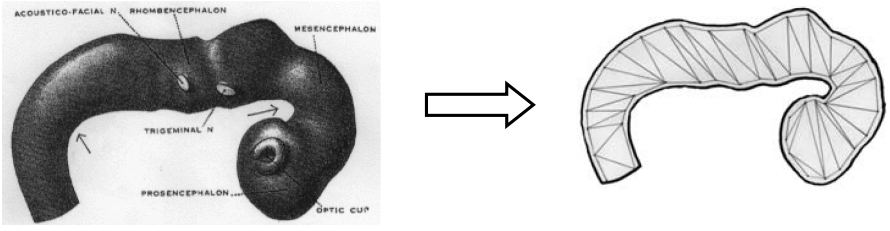

Fig. 2. The conversion of drawing human embryo brain to central skeleton

prosencephalon. The next step is to calculate the central line that will be used as a base to define the thickness of the model along the line forming the tubular object. Central line passes through the center of central skeleton, connecting the mid points of vertical edges of a triangular strip.

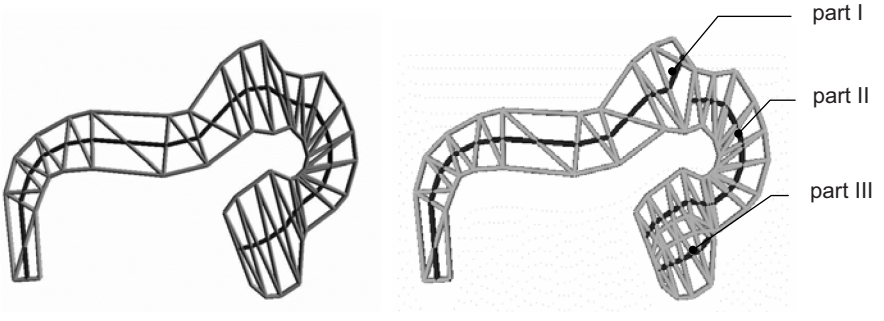

Fig. 3. Dividing the central skeleton to 3 parts. The line in the middle of the central skeleton is called central line.

4.3 Brain: Skeleton

By adding the thickness to 2D central skeleton the 3D skeleton of the model is obtained. Multiple number of copies of central skeleton are slightly scaled and shifted to left and right sides of central skeleton. By this way the cross sections are produced which are then connected to form the tubular skeleton, see Figure 4:

- Each of side skeletons is scaled to fit the ellipses whose center is on the central line. Radius a of the ellipse is a distance to the central line from the border of the central skeleton. Radius b follows the equation, $b = \alpha a$, where α is a ratio parameter.
- As next step, for a given θ the side skeletons are translated by distance $t = c \cos \theta$, where c is known from parametric equation of ellipse shown in Figure 5.

– Finally, side skeletons are connected with a central skeleton or with other side skeletons by a triangular mesh.
– After erasing all interior triangular patches we obtain multiple tubular shapes forming together the entire skeleton of the brain.

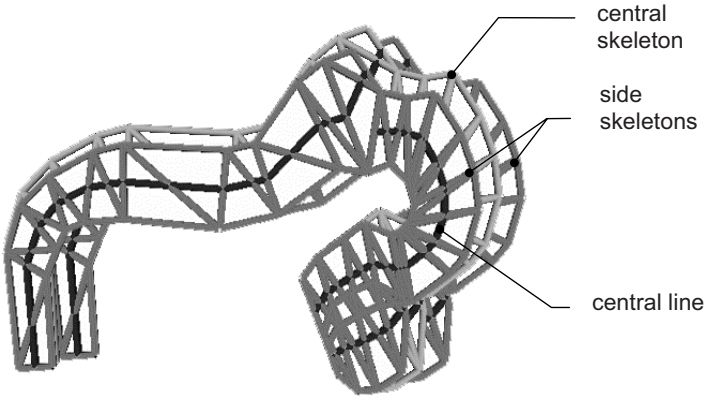

Fig. 4. Adding the thickness by scaling and shifting the central skeleton

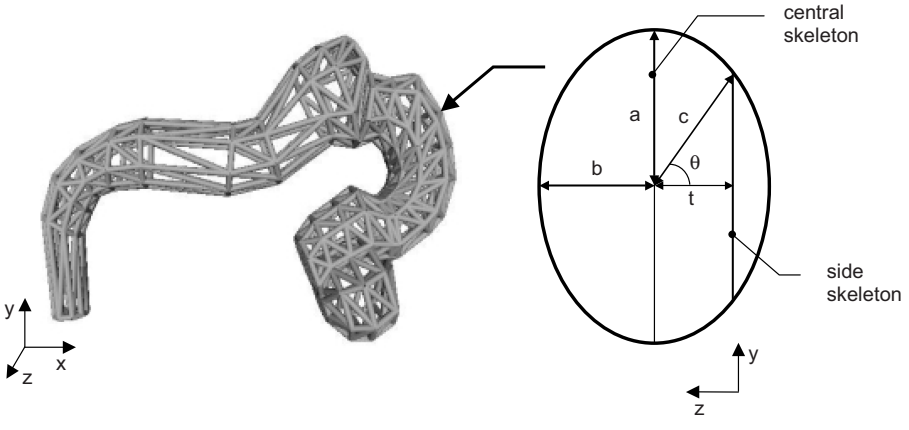

Fig. 5. A 3D skeleton for 36 days old human embryo brain

4.4 Model of the Human Digestive System

To approximate the shape of an organ while considering the speed and direction of cell growth at the same time, we group the entire set of cells into a number of cylindrical bunches (clusters). Thus, the skeleton of the organ is defined by a

chain of linear segments passing through the cluster centers, see Fig. 6. Organ growth can then be modeled by the growth of the line skeleton, and variations in shape thickness during the growth process can be captured by variations in cylinder size. When a cylinder changed in size, it was understood that the organ cells grew in the directions emanating from the cluster center. Similarly, when the skeleton segment underwent changes in length, it was understood that the cells included in two adjoined clusters grew in directions parallel to this segment.

Taking into account the development, the organs were divided into physiological parts having different speed and direction of growth to suite the animation purposes. The physiological parts of the intestine system are shown in Fig. 7 and marked I, II and III for stomach, marked IV for small intestine, marked VII for large intestine, marked V for appendix, and marked VI for vitteline duct. While refering to Langman's embryology [11] we collected data that are shown in Table 1. For each available embryo age (developmental stage) of large intestine its mean thickness and skeleton length are listed. Statistical data for a human embryo stomach have already been summarized by Ďurikovič *et al.*[2].

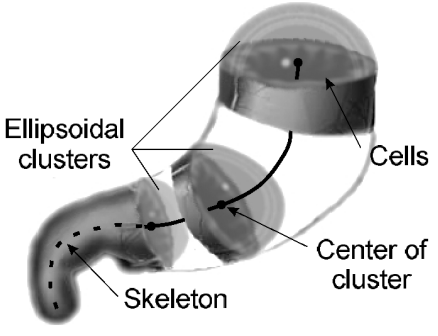

Fig. 6. Skeleton of the organ and the clusters

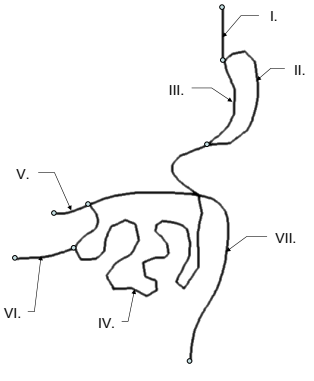

Fig. 7. Physiological parts represented with line skeleton

Table 1. Shape measurements of large intestine, physiological part no. IV

Embryo age (day)	Length (mm)	Thickness (mm)	
28	2.76	0.30	herniation
49	15.58	0.45	
58	19.49	0.52	
70	21.77	0.61	reduction
83	24.04	0.82	
113	28.62	1.00	fixation

The organs, at this preprocessing stage, were divided into physiological parts having different speeds and directions of growth to suite the animation purposes.

4.5 Digestive System: Skeleton

The topology of the digestive system is expressed by a tree structure and the development of the tree-like structure can be easily modeled with an algebraic L-system [12,13]. An L-system formalism was proposed by Lindenmayer [14], and the method has been used as a general framework for plant modeling. The L-systems are extended to by introducing continuous global time control over the productions, stochastic rules for the capture of small variations, and explicit functions of time used to describe continuous aspects of model behavior, in addition to differential equations.

In some cases it is convenient to describe continuous behavior of the model using explicit functions of time rather then differential equations. For example, global shape transformations varying over time require a large and complicated system of differential equations, while only few explicit functions of time are sufficient for the description of these transformations.

4.6 Cell Model

Let's move to a micro structure of muscle cell structures on the organelle level. We present a modeling concept based on the theory of implicit surfaces that allows for creation of a realistic infrastructure of the micro-world of muscle cells. From the viewpoint of geometry, the structure of living cells is given by the three-dimensional organization of their numerous intracellular organelles of various sizes, shapes and locations.

4.7 Cell: Central Skeleton

The initial step involves creation of the central skeleton of the cell, which is represented by a system of parallel cross-sectional graphs (c-graphs) distributed along the longitudinal axis. We define the c-graph as a continuous planar graph which divides the plane in a finite number of closed non-intersecting polygons. Then we exploit the two-dimensional c-graphs to create the myofibrillar system

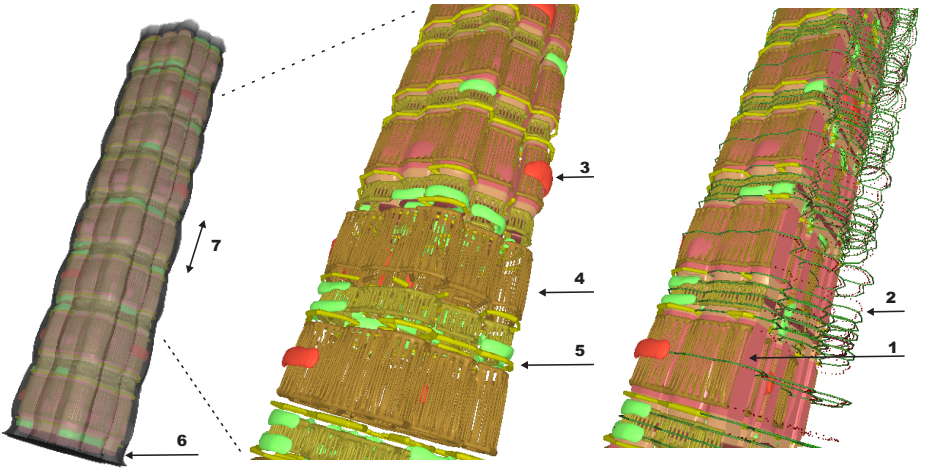

Fig. 8. An example demonstrating eight consecutive sarcomeres of a muscle cell (left). For better clarity, the sarcolemma is hidden and, also, the bottom part of the myofibrillar system is clipped of by a transversal plane (middle). The complex system of underlying skeletons is made visible by clipping with a longitudinal plane (right). The myofibrillar system (1) is defined by means of c-graphs (2). The remaining organelles include mitochondria (3), sarcoplasmic reticulum (4), t-tubules (5) and sarcolemma (6); given in the basic repetitive unit, sarcomere (7).

by means of the F-rep representation of polygons and interpolation. For better clarity, this concept is demonstrated in Figure 8.

In the following subsections we propose approaches for creation of the most complex structures of muscle cells, reticulum and mitochondria.

4.8 Cell: Skeleton

The basic modeling object at this step is a set of seed points distributed in a system of several cross-sectional planes as shown in Figure 9a. Let $\mathbf{S} = \{s_1, s_2, \ldots, s_n\}$ stand for the set of seeds in one crossection. Each seed produces an implicit circle f_i with an appropriate radius. The whole contribution of $\mathbf{S}$ is represented by CSG union:

$$f(\mathbf{S}) = \bigcup_{s \in \mathbf{S}} f_s. \tag{3}$$

Similarly, we define the set $\mathbf{R}$ of seeds in a neighboring crossection. To create a smooth junction between shapes $f(\mathbf{S})$ and $f(\mathbf{R})$ we apply an interpolation method.

Assume that both shapes (sets of implicit circles) contain a set of control points, $\mathbf{P} = \{p_1, \ldots, p_n\}$ for the function $f(\mathbf{S})$ and $\mathbf{Q} = \{q_1, \ldots, q_n\}$ for the function $f(\mathbf{R})$. Moreover, vectors of correspondence are specified between these

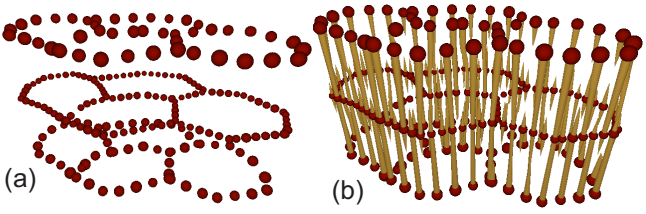

Fig. 9. (a) Seeds (here represented by the red spheres) are distributed in sets of parallel planes. (b) A classical interpolation technique results in non-interconnected segments.

points, $\mathbf{C}_P = \{q_1 - p_1, \ldots, q_n - p_n\}$ and $\mathbf{C}_Q = \{p_1 - q_1, \ldots, p_n - q_n\}$. The set $\mathbf{C}_P$ is attached to the set $\mathbf{P}$, and the set $\mathbf{C}_Q$ is attached to the set $\mathbf{Q}$. Now, we create two weighting displacement functions ϕ^p and ϕ^q, which represent transformations of the given shapes in the directions defined by the vectors of $\mathbf{C}_P$ and $\mathbf{C}_Q$. The weighting displacement functions are defined by

$$\begin{aligned} \phi^p(\mathbf{x}) &= \mathbf{x} + h_1(t)d_1(\mathbf{x}) \\ \phi^q(\mathbf{x}) &= \mathbf{x} + h_2(t)d_2(\mathbf{x}), \end{aligned} \tag{4}$$

where $h_1(t)$, $h_2(t)$ represent weighting proportions within the interval $< 0, 1 >$, and $d_1(x)$, $d_2(x)$ represent interpolation of control points given by vectors of $\mathbf{C}_P$ and $\mathbf{C}_Q$. To interpolate the displacement d_1, d_2 we adopt volume splines—the so-called thin-plate function [15,16]. The weighting factors h_1 and h_2, i. e. functions that specify the size of control point displacements, are defined as

$$\begin{aligned} h_1(t) &= (1 - t^a)^b \\ h_2(t) &= 1 - h_1(t), \end{aligned} \tag{5}$$

where the parameters a, b modify the slope and curvature of the transition (Fig. 10a).

To create the required smooth transformation without gaps, the linear interpolation is modified by the displacement functions, Eqs. 4:

$$F_{lt} = (1 - t)f(\mathbf{S})(\phi^p(\mathbf{x})) + tf(\mathbf{R})(\phi^q(\mathbf{x})) + aw_3(t), \tag{6}$$

where $aw_3(t)$ is the additional blending term used to fine-tune interconnection of shapes by adding material primarily in the central part of the interpolation region. The parameter a stands for the amount of blending and the weighting function $w_3(t)$ is defined as

$$w_3(t) = (1 - (2t - 1)^c)^d, \tag{7}$$

where the parameters c, d modify the slope and the curvature (Fig. 10b).

A result of this approach with three sets of seeds defined in three parallel planes is depicted in Figure 11a.

Fig. 10. (a) Weighting functions h_1 and h_2. (b) The weighting function w_3 has the maximum in the middle.

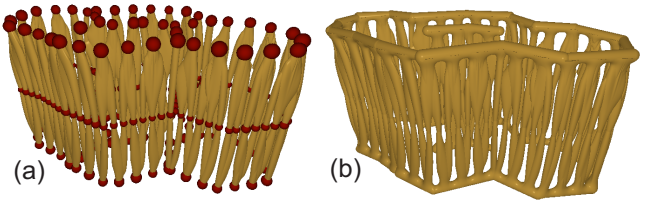

Fig. 11. Modeling of sarcoplasmic reticulum. (a) The final warping interpolation provides gap free interconnections. (b) The smooth junction between terminal cisterns and tubes is obtained by the blended union.

The second step in the building process is formation of terminal cisterns. These cylindrical shaped objects form a smooth junction to systems of longitudinal tubules. Terminal cisterns are created as blended union of implicit cylinders. Their underlying line segments are obtained by connecting the seeds in the bottom most and the top most plane of the system of crossectional planes, see Figure 11b.

4.9 Cell: Mitochondria

In order to capture the varying elliptical shape of mitochondria, we use implicit sweep objects. The basic components of sweep objects are a 2D sweep template and a 3D sweep trajectory. Here, the 2D template is a 2D implicit ellipse with variable dimensions. Figure 12 demonstrates such a mitochondrion defined by a trajectory specified by means of spline control points.

5 Organ Growth

Continuous processes such as the elongation of skeleton segments, and growth of cell clusters, over time can easily be described by the growth functions. Growth functions can be then included into algebraic L-systems as explicit functions or differential equations. Growth is often slow initially, accelerating near the maximum stage, slowing again and eventually terminating. A popular example

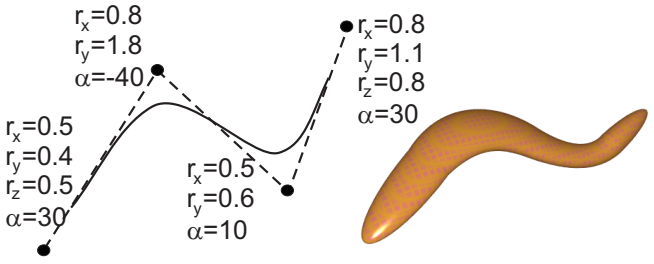

Fig. 12. The curve, represented as a quadratic B-spline, is created from the control points, where each has assigned corresponding radii and rotation angles (left). Note end control points have specified also z radius for 3D ellipsoid. The resultant sweep object is depicted on the right.

of the growth function [17] is the *logistic* function which is a solution to the following differential equation

$$\frac{\partial r}{\partial t} = p\left(1 - \frac{r}{r_{\max}}\right) r \equiv g_{r_{\max},p}(r). \tag{8}$$

Logistic function monotonically increases from initial value r_0 to r_{max} with growth rates of zero at start and end of time interval $[T_0, T]$. It is an S shape function with a steep controlled by a parameter p.

The details of the L-system tables have been described by Durikovic [13]. He has described the skeleton elongation, the global bending of the skeleton parts, dynamics of skeleton structures, and growth functions.

6 Shape from Skeleton

The measured organ models discussed in previous section were divided into physiological parts, at preprocessing stage, having different speed and direction of growth to suit the animation purposes. A single physiological part has the shape defined by the skeleton based F-rep. The skeleton of the physiological part can be animated directly by a key-frame animation or we can use a sophisticated methods to simulate the skeleton growth based on L-system or the dynamic L-system.

6.1 Brain Shape

A smooth convolution surface defined over the triangular mesh of tubular skeleton creates the model of embryo brain. In order to create brain model with convolution surfaces, we use HyperFun[1,9] as modelling library and POV-Ray[8] as rendering software. HyperFun command hfConvTriangle generates convolution surface over the triangles which suites our problem. Let us discuss all parameter settings for one particular example, the *stage3* human embryo brain shown

in Figure 13. The convolution kernel width is set to $s = 0.5$ and iso-potential threshold value is $T = 0.6$. The ration parameters of brain thickness have been set to $\alpha = 1.0$ at parts I and II and to $\alpha = 1.2$ at part III. Nice blending during the animation can be guarantied by blend-union operation between three parts of this model using the HyperFun command hfBlendUni. The blending parameters $a_1 = a_2 = a_3 = 0.2$ are used for both gluing parts I, II and parts II and III, respectively.

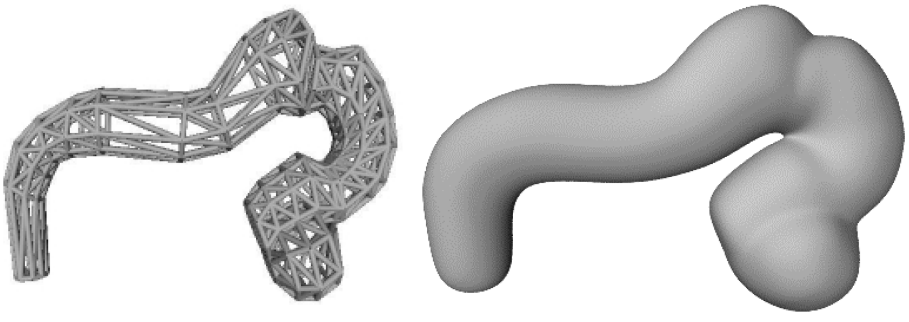

Fig. 13. Stage3 human embryo brain. Left: 3D tubular skeleton, right: entire brain model, defined by function representation.

6.2 Shape of the Digestive System

We represent the smooth shape of the digestive system in a compact way by piecewise linear skeleton and locally defined convolution cylinders along each linear segment of a skeleton. Thus, the resulting smooth tubular surface is represented by a real function as the blend union operation between many convolution cylinders. The shape of a convolution surface can be varied in several ways: by varying the skeleton, by varying the thickness of convolution cylinders with parameter s from Eq. 9, and by the iso-potential threshold value T:

$$f_i(X) = \int_{V_i} \frac{1}{(1 + s^2 r^2(v))^2} dv - T. \tag{9}$$

For example, the small and large intestines monotonically increase their thickness which can be modeled with the monotonically decreasing parameter s as seen for the six developmental stages of intestine in Table 2.

Thickness. As was already mentioned, the increasing thickness of convolution cylinders distributed along the skeleton segments is given by monotonically decreasing the width parameter s in time as shown in Table 2. We will transform the solution of Eq. 10, $\hat{s}$, that monotonically increases from 0.01 to 0.16 over the time interval $[28, 120]$ into a monotonically decreasing function s by Eq. 11,

Table 2. Convolution parameters for thickness of small and large intestine

	Intestine			
Embryo age (day)	Small		Large	
	s	T	s	T
28	0.45	0.2	0.69	0.25
49	0.42	0.2	0.67	0.25
58	0.40	0.2	0.63	0.25
70	0.35	0.2	0.60	0.25
83	0.32	0.2	0.57	0.25
113	0.29	0.2	0.54	0.25

where $s_{max} = 0.7$:

$$\frac{\partial \hat{s}(t)}{\partial t} = g_{0.16,0.003}(\hat{s}), \quad \hat{s}(28) = 0.01 \tag{10}$$

$$s(t) = s_{max} - \hat{s}(t). \tag{11}$$

Function $s(t)$ is the growth function controlling the thickness of large intestine with a good approximation of data from Table 1. The graph of the growth function over the time is shown on right of Fig. 14.

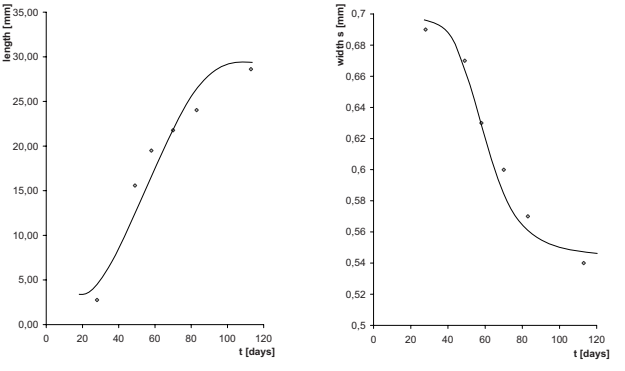

Fig. 14. Graphs of growth functions. Left) Total length of large intestine in time. Right) Change of width parameter s in time, see Eq. 9.

7 Results

Few frames from animation of *Organ growth* show the embryo stomach and brain described by embryo age and the real size scale bar, see Figures 15, 16.

Shown in Fig. 17 are several frames from a generated animation simulating digestive growth based on the proposed L-system using the above growth functions. The environment forces and self collision were handled by the spring

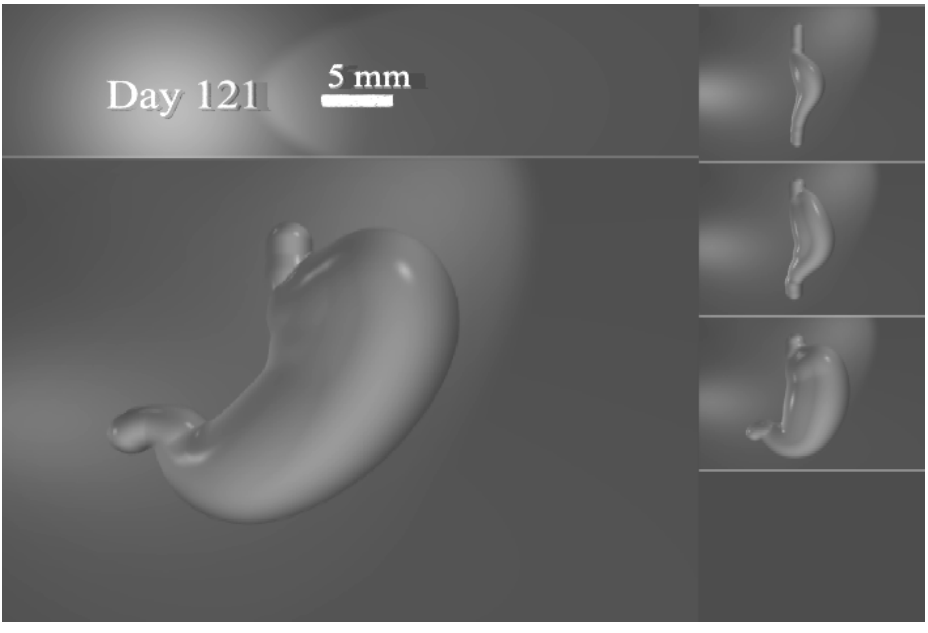

Fig. 15. A single frame from the human embryo stomach animation

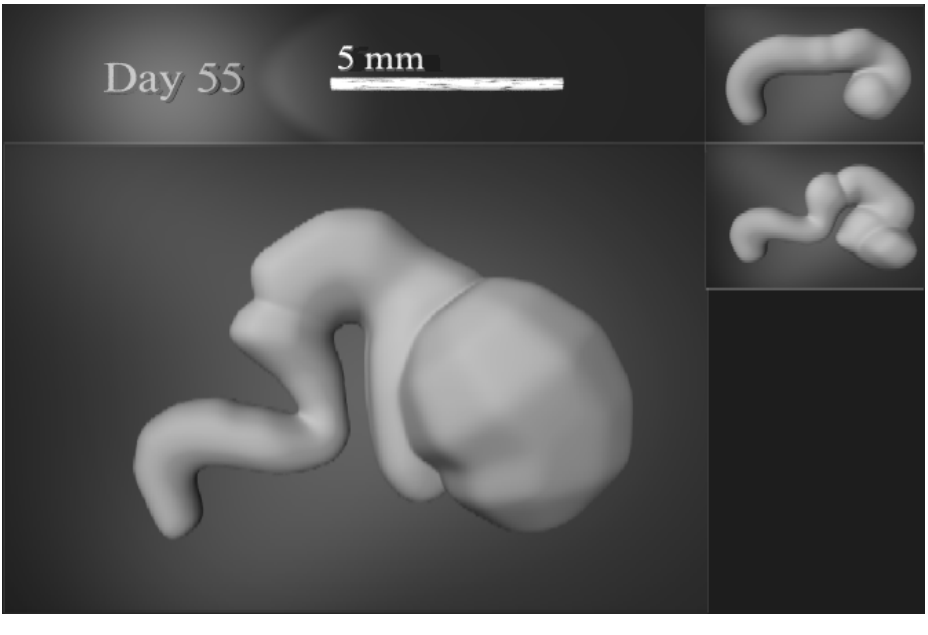

Fig. 16. A single frame from the human embryo brain animation

representation of results obtained from L-system. The shape of the digestive system shown in this figure undergoes global bending transformation and deformations resulting from gravity, animator intervention (looping process), and collision. Some of the intermediate shapes in Fig. 17 have disjoined elements due to aliasing in the implicit polygonizer that has difficulties to find a mesh for long thin structures.

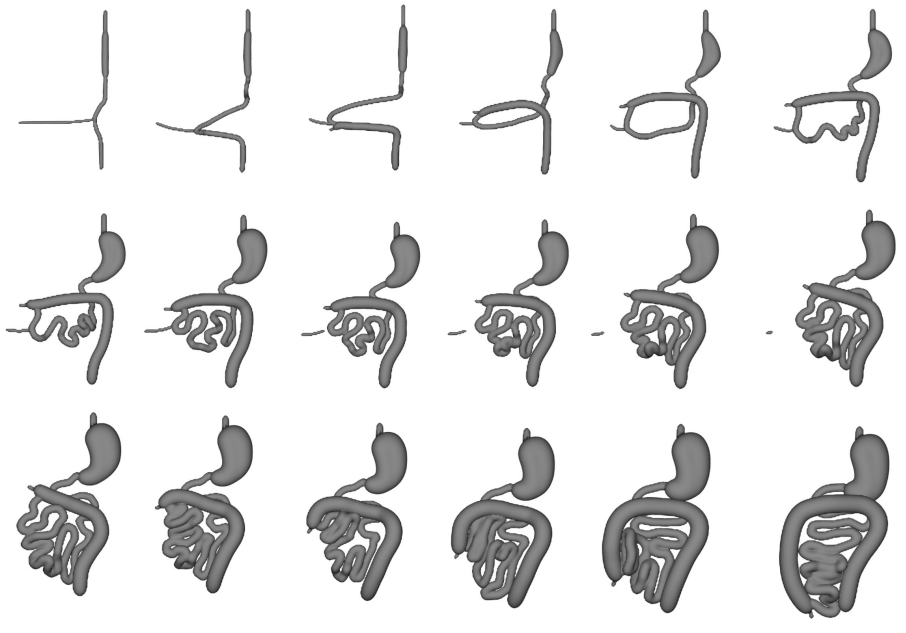

Fig. 17. Development of a human embryo digestive system with proposed method taking into account the skeleton dynamics and growth functions in algebraic L-system. Function representation is used to define a smooth shape. Indicated stages from left to right represent 28, 34, 40, 49, 52, 58, 64, 70, 76, 79, 83, 94, 101, 107, 110, and 113 days of animation sequence.

8 Conclusions

We have presented a method for simulation of the growth of human embryo digestive system. The method uses the shape calculated based on F-rep using isosurfaces generated by skeleton segments, which provides a smooth and compact representation of the surface usable for complex animations. We proposed a method in which the organ growth and global bends are separate processes. The differential growth functions are introduced for an algebraic L-system which efficiently control the elongation of skeleton segments.

We succeeded to model structure of living cells, virtual human embryo organs, namely brain, stomach and digestive system using convolution surfaces and functional representation. The growth animation of a stomach was generated for all 9

months of development while the brain growth animation was generated for first 4 months of embryo development. The advantage of skeleton based approach is that it avoids the the topology artifacts that can occur when using the nonlinear interpolation between two defining functions of F-rep models. Variable speed of growth and shape thickness is successfully modelled by convolution plus or blending union between model parts.

We have proposed the skeletons consisting of triangular patches which gives us the opportunity to define the flat shapes like pillow, refer to the brain model.

Acknowledgements

Authors wishes to thank Mineo Yasuda from Medical School of Hiroshima University for sharing the knowledge as an embryologist. The authors are grateful to Laboratory of Cell Morphology at the Institute of Molecular Physiology and Genetics, Slovak Academy of Sciences. The images were rendered by the POVRay ray-tracing program programmed by POVRay Team. This research was supported by a Marie Curie International Reintegration Grant within the 6^{th} European Community Framework Programme EU-FP6-MC-040681-APCOCOS.

References

1. Ďurikovič, R., Kaneda, K., Yamashita, H.: Imaging and modelling from serial microscopic sections for the study of anatomy. IEEE Medical & Biological Engineering & Computing 36(3), 276–284 (1998)
2. Ďurikovič, R., Kaneda, K., Yamashita, H.: Animation of biological organ growth based on l-systems. Computer Graphics Forum (EUROGRAPHICS 1998) 17(3), 1–13 (1998)
3. Smith, C., Prusinkiewicz, P.: Simulation modeling of growing tissues. In: Proceedings of the 4th International Workshop on Functional-Structural Plant Models, pp. 365–370 (2004)
4. Felkel, P., Fuhrmann, A., Kanitsar, A., Wegenkittl, R.: Surface reconstruction of the branching vessels for augmented reality aided surgery. In: Proceedings of the Biosignal, pp. 252–2549 (2002)
5. Tsingos, N., Bittar, E., Gascuel, M.P.: Implicit surfaces for semi-automatic medical organ reconstruction. In: Earnshaw, R., Vince, J. (eds.) Computer Graphics, development in virtual environments, proceedings of Computer Graphics International 1995, Leeds, UK, May 1995, Academic Press, London (1995)
6. Tait, R., Schaefer, G., Kühnapfel, U., Çakmak, H.K.: Interactive spline modelling of human organs for surgical simulators. In: 17th European Simulation Multiconference, Nottingham Trent University, Nottingham, England, pp. 355–359 (2003) ISBN 3-936150-25-7
7. Amrani, M., Jaillet, F., Melkemi, M., Shariat, B.: Simulation of deformable organs with a hybrid approach. In: In Proceedings of the Revue Int. d'infographie et de la CFAO (2001)
8. Leymarie, F.F., Kimia, B.B.: Shock scaffolds for 3d shapes in medical applications. In: DIMACS Workshop on Medical Applications in Computational Geometry, DIMACS Center, Rutgers University, Piscataway, NJ (2003)

9. Attali, D., Montanvert, A.: Semi-continuous skeletons of 2D and 3D shapes in C. World Scientific, New York (1994)
10. Pasko, A., Adzhiev, V., Sourin, A., Savchenko, V.: Function representation in geometric modeling: concepts, implementation and applications. The Visual Computer 11(8), 429–446 (1995)
11. Sadler, T.W.: Langman's medical embryology, 7th edn. Williams & Wilkins, New York (1995)
12. Mech, R., Prusinkiewicz, P.: Visual models of plants interacting with their environment. In: SIGGRAPH, pp. 397–410 (1996)
13. Ďurikovič, R.: Growth simulation of digestive system using function representation and skeleton dynamics. International Journal on Shape Modeling 10(1), 31–49 (2004)
14. Prusinkiewicz, P., Lindenmayer, A., Hanan, J.: Development models of herbaceous plants for computer imagery purposes. In: SIGGRAPH 1988: Proceedings of the 15th annual conference on Computer graphics and interactive techniques, pp. 141–150. ACM Press, New York (1988)
15. Duchon, J.: Splines minimizing rotation-invariant semi-norms in Sobolev spaces. In: Schempp, W., Zeller, K. (eds.) Constructive Theory of Functions of Several Variables. Lecture Notes in Mathematics, vol. 571, pp. 85–100. Springer, Heidelberg (1977)
16. Savchenko, V., Pasko, A.: Transformation of functionally defined shapes by extended space mappings. The Visual Computer 14(5-6), 257–270 (1998)
17. Edelstein-Keshet, L.: Mathematical models in biology. McGraw-Hill, New York (1988)